Acta Cryst. (1996). D**52**, 30–42

Methods Used in the Structure Determination of Bovine Mitochondrial F_1 ATPase*

J. P. ABRAHAMS AND A. G. W. LESLIE

MRC Laboratory of Molecular Biology, Hills Road, Cambridge CB2 2QH, England

(Received 2 June 1995; accepted 28 June 1995)

Abstract

With a size of 372 kDa, the F_1 ATPase particle is the largest asymmetric structure solved to date. Isomorphous differences arising from reacting the crystals with methyl-mercury nitrate at two concentrations allowed the structure determination. Careful data collection and data processing were essential in this process as well as a new form of electron-density modification, 'solvent flipping'. The most important feature of tnis new procedure is that the electron density in the solvent region is inverted rather than set to a constant value, as in conventional solvent flattening. All non-standard techniques and variations on new techniques which were employed in the structure determination are described.

1. Introduction

The biological regeneration of ATP from ADP and inorganic phosphate in mitochondria and chloroplasts is driven by a proton gradient across the inner membrane of the former or the thylakoid membrane of the latter organelle. This electrochemical potential is created by respiratory or photosynthetic processes. Its conversion into the chemical potential stored by ATP is catalysed by ATP synthase, a multiprotein assembly partially embedded in these membranes. A similar system exists in bacteria and archaea, which can both create and utilize a proton gradient while consuming or synthesizing ATP. The synthase particle can be dissociated into a membrane domain, which contains a proton channel, and a soluble domain, called F_1, which is an ATPase. The soluble domain isolated from bovine mitochondria contains three regulatory α subunits (55 kDa each), three catalytically active β subunits (52 kDa each) and single copies of the γ, δ, and ε subunits (30, 15 and 5.6 kDa, respectively). The presence of single copy subunits in F_1 ATPase indicates an asymmetry which manifests itself in the biochemical properties of the particle, as reviewed by Boyer (1994). One of the intriguing aspects of its enzymology is that the allosterically coupled active sites cycle sequentially, rather than simultaneously through the different states of catalysis.

The structure of bovine mitochondrial F_1 ATPase was solved to 2.8 Å resolution (Abrahams, Lutter, Leslie & Walker, 1994) from crystals grown in space group $P2_12_12_1$ with a unit cell of $284.2 \times 107.8 \times 139.7$ Å and one particle per asymmetric unit (Lutter *et al.*, 1993).

* A report of the meeting at which this paper was presented is published on pages 228–234 of this issue.

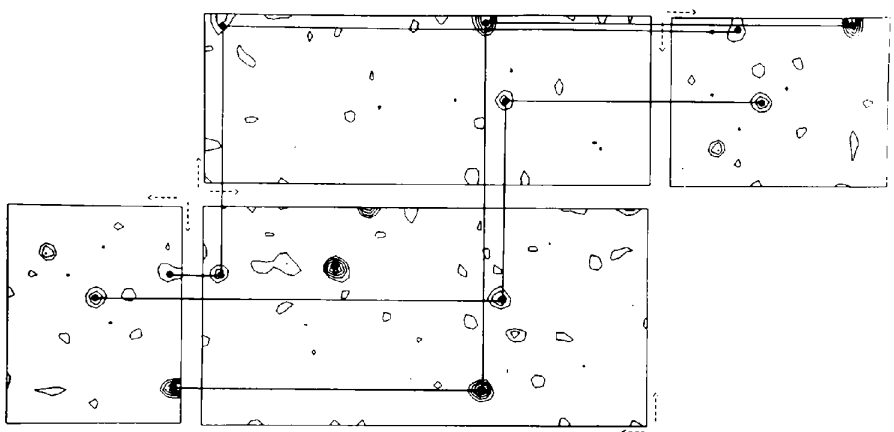

Fig. 1. Harker sections at 6.5 Å resolution contoured at 1.5σ of a difference Patterson of F_1 ATPase, ranging from 0 to 0.5 of the fractional unit cell, after soaking the crystals for 16 h in 0.2 m*M* methyl-mercury nitrate. The direction of the axes are indicated at the origins of the Harker sections. Note that one of the sections is duplicated. In the space group $P2_12_12_1$, cross-peaks of crystallographically related heavy-atom sites can be connected as indicated. The additional peaks in the difference Patterson, including the remaining peaks in the Harker sections, could be explained by the constellation of the three sites indicated.

With a total molecular weight of 372 kDa, this is the largest asymmetrical structure determined to near atomic resolution to date. The biological implications of the structure have been discussed previously and here we give a detailed account of the methods used for its solution.

2. Methods

2.1. *Reduction of non-isomorphism*

The crucial step in obtaining crystals that diffracted to beyond 3 Å rather than to about 7 Å was to strip the F_1 ATPase particle of all bound nucleotides and then add the non-hydrolyzable ATP analogue AMPPNP (Lutter *et al.*, 1993). Initially, these native crystals were found to be non-isomorphous with one another. However, we discovered that the non-isomorphism could be greatly reduced, although not entirely eliminated, by soaking native crystals in a solution containing 10 μM of the alternative substrate ADP and 250 μM of AMPPNP. This experiment was inspired by the observation that preparations of commercially available AMPPNP can be contaminated with variable amounts of AMPPN and ADP. Subsequently, crystals grown in a mother liquor containing both 250 μM AMPPNP and 5 μM ADP were shown to be even more isomorphous. The structure reveals that four of the six nucleotide-binding sites are filled with AMPPNP, while one site is filled with ADP and the remaining site is empty. This provides a rational explanation for the effect of inclusion of ADP on the reproducibility of the crystals.

However, because problems with non-isomorphism could not be eliminated entirely, for each derivative data set with a resolution higher than 6.5 Å, a corresponding native data set was collected from crystals of the same batch which had been soaked under identical conditions in the stabilizing solution, but without the heavy-atom compound.

Multiple crystals were needed for most high-resolution data sets, since flash-freezing trials resulted in an intolerable increase in mosaic spread of the crystals, and in unreproducible changes of their cell dimensions.

2.2. *Crystal mounting and data collection*

Crystals of F_1 ATPase are fragile and decay quite rapidly when irradiated. We found that the lifetime of the crystals could be prolonged, and that the mosaic spread could be minimized by adopting a special mounting technique. First, the crystal is introduced into a tapered glass capillary which is filled with the stabilizing solution. The crystal drops down under gravity until it wedges itself in the tapered end, and the capillary is sealed. Because the crystal remains bathed in the stabilizing solution, it is kept fully hydrated at all times and the effects of sudden temperature changes are reduced. Unless the crystal is plate-like, the volume of stabilizing solution

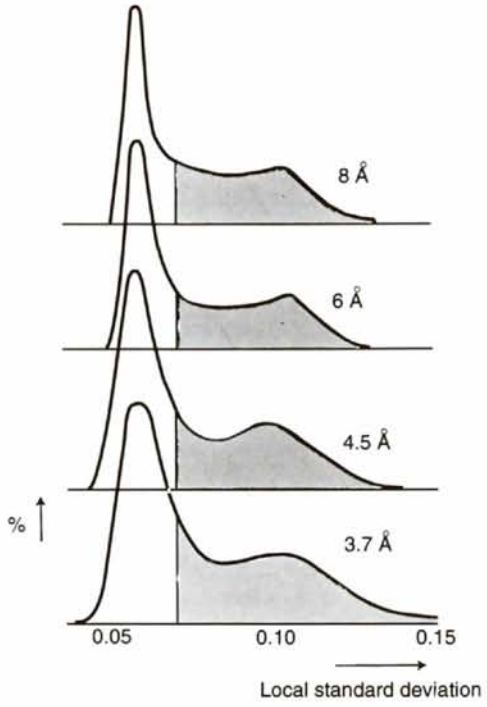

(*a*)

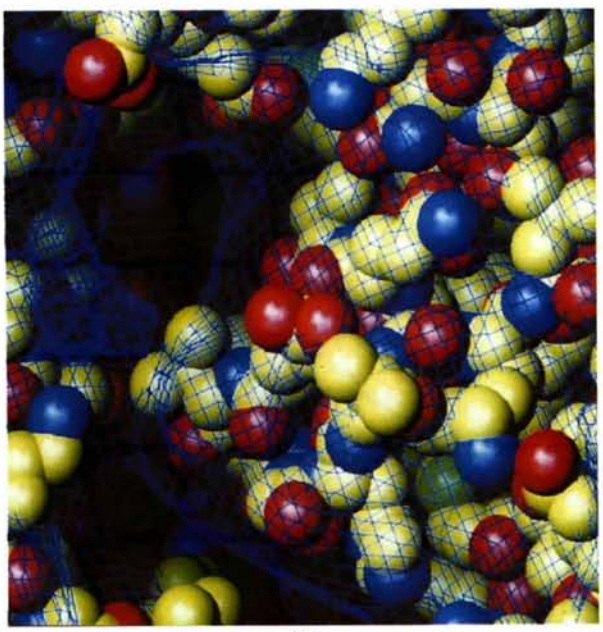

(*b*)

Fig. 2. (*a*) Histograms of the local standard deviation from the mean density of figure-of-merit weighted MIR maps of F_1 ATPase. The local standard deviation was determined within spheres with radii as indicated. The solvent content of the crystals was calculated to be 54%, and the top 46% of the histograms are highlighted. The bimodality of the histograms reflects the solvent content, even when relatively short integration radii are used. (*b*) Superposition of a CPK model of a small part of the refined model of F_1 ATPase, containing a tunnel towards one of the active sites, with the solvent mask as derived from the initial figure-of-merit weighted MIR map, calculated using a 4.5 Å integration radius and a solvent content of 50%.

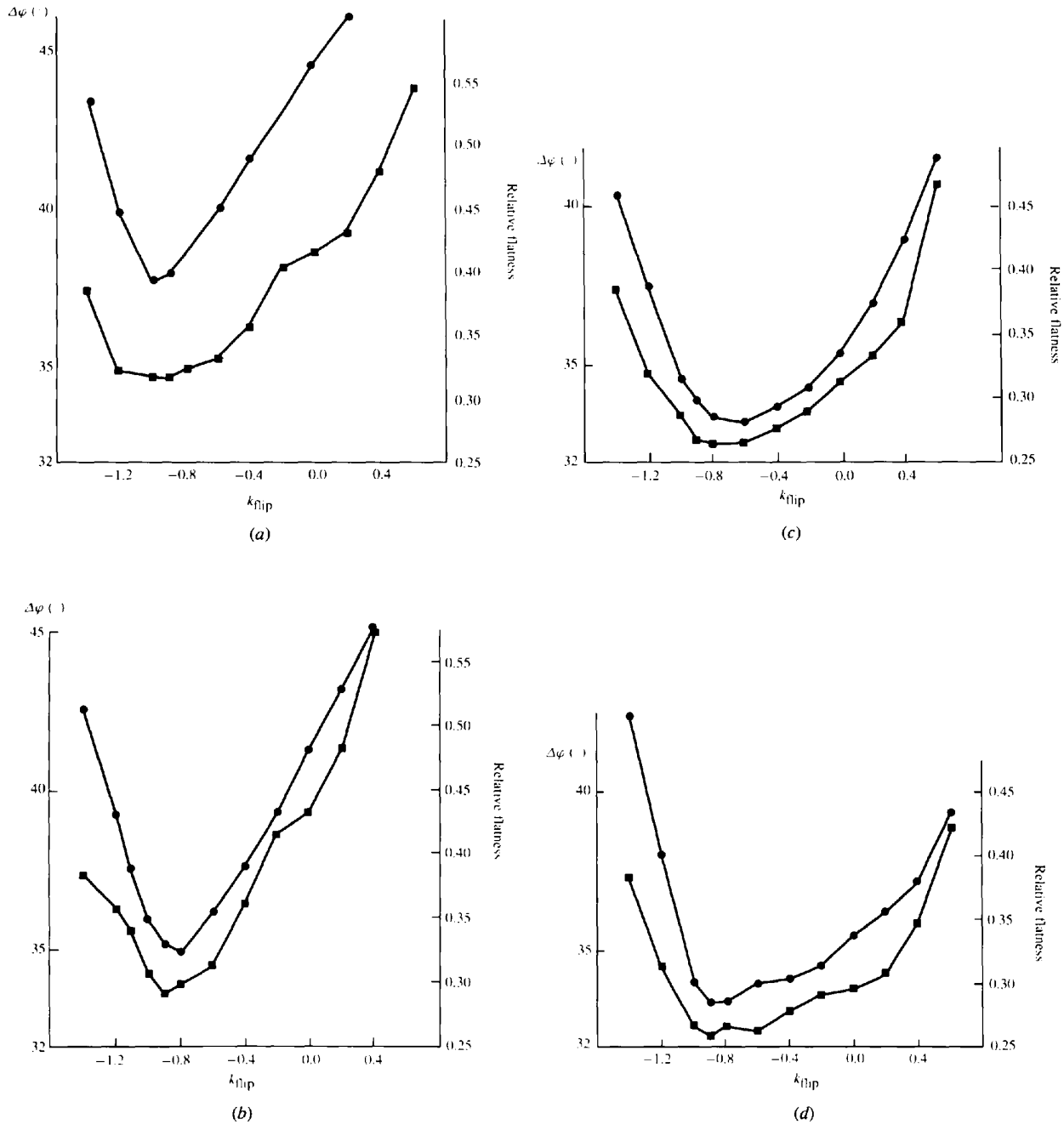

Fig. 3. The effect of solvent flipping on reducing the phase error (denoted by filled circles) and on the ratio between the standard deviations of the electron density within the reporter sphere and of the protein region (the 'relative flatness', denoted by filled squares). The reporter sphere encompasses a volume of solvent which was not modified throughout the density-modification procedure. On every cycle, the solvent mask was determined from a map of the local standard deviation of the electron density within a radius of 3.7 Å, assuming a solvent content of 50%. The density within the solvent mask was modified relative to the mean of the density map by a factor indicated on the horizontal axis on cycles 1 to 19, and the solvent was flattened on cycle 20. In all cases the lowest (except in *b*) and highest 2% of the protein density were truncated. (*a*) No non-crystallographic symmetry was imposed. (*b*) No non-crystallographic symmetry was imposed and the lowest 20% of the electron density within the protein mask was truncated by setting the density of gridpoints within the protein region lower than the cut-off value to this constant. (*c*) Strict non-crystallographic symmetry was imposed, using separate masks and symmetry operators for each of the three domains of the α and β subunits. However, the nucleotide-binding domain of the empty β subunit was not averaged, since this domain is very different from the corresponding domains of the other 3 subunits. See also Abrahams *et al.* (1994) for a description of the asymmetry of the particle. (*d*) Permissive threefold non-crystallographic symmetry was imposed, weighted according to the probability that the observed differences between symmetry-related parts are accidental (see text).

surrounding the crystal is small so that the background scatter is reduced. This mounting procedure minimizes handling of the crystal and eliminates any stresses due to the removal of excess mother liquor, resulting in a low mosaic spread, typically in the order of 0.1 to 0.2°. Provided that a horizontal rotation axis is used and that the tip of the capillary always points slightly downward, slippage of the crystal during data collection is minimal.

Another potential advantage of the described mounting procedure is that the crystal can quite safely be supercooled by 5 to 10 K below the freezing temperature of the stabilizing solution. However, care needs to taken when the solution is virtually saturated with a small heavy-atom compound: when a decrease in temperature causes precipitation, the resulting microcrystals act as nucleation sites, and the super-cooled solution freezes instantaneously. To avoid this problem, all data were collected at 268 K.

For data collection, the crystallographic axes were offset from the rotation axis by at least 15° at all times. In this way, even small wedges of data cover significant parts of the unique volume of reciprocal space. The procedure, therefore, usually increases the overlap between data from different crystals, which facilitates identification of non-isomorphism. In addition, it eliminates the cusp region that would result from rotation about a crystallographic axis.

All data were collected on MAR Research image-plate detectors. In the laboratory, Cu $K\alpha$ radiation was generated by an Elliot GX13 rotating anode with a 100 μm line focus and double mirror collimation (Charles Supper Ltd). In this case, the efficiency of data collection was increased by the use of a helium path between the crystal and the detector. The path consisted of a cheap plastic garbage bag, inflated with slightly pressurized helium. These bags are virtually transparent to X-rays due to their thickness of only 20 μm, and they are practically helium tight.

In order to collect a complete native data set with a resolution of 2.8 Å, synchrotron radiation was essential. It was necessary to merge data from 17 crystals, since no more than 3° of data could be collected from any position of a crystal without inducing unacceptable radiation damage. The angular width per frame was chosen to be 0.3° in order to minimize spatial overlap and to reduce the X-ray background. All synchrotron data were collected at the SRS in Daresbury, England. Derivative data from crystals soaked in 0.2 and 1 m*M* methyl-mercury nitrate were collected to resolutions of 3.2 and 3.5 Å, respectively, at wavelengths of 0.90 and 0.92 Å. For technical reasons, no attempt was made to increase the anomalous signal of the derivative data sets by tuning the wavelength of the X-ray beam.

All data were processed with *MOSFLM* (Leslie, 1992) and programs from the *CCP*4 suite (Collaborative Computational Project, Number 4, 1994). The algorithms in *MOSFLM* were optimized to obtain the highest possible data quality, particularly with regard to resolving adjacent reflections along the 284 Å long crystallographic '*a*' axis.

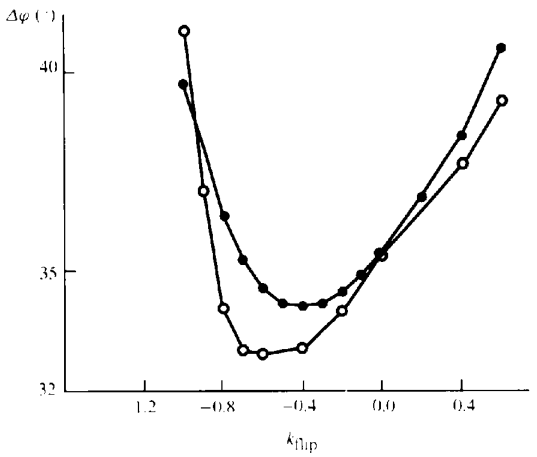

Fig. 4. The effect of overshifting the structure-factor changes resulting from non-crystallographic averaging and solvent flattening. The horizontal axis indicates the multiplier by which the structure-factor shift between subsequent cycles of the density-modification procedure is scaled before subtracting it from the modified structure factor. In the absence of non-crystallographic averaging, this multiplier is equivalent to k_{flip} in Fig. 3.

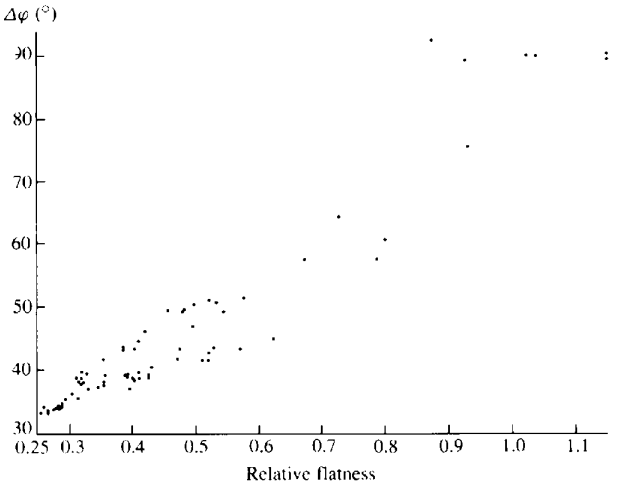

Fig. 5. The correlation between the flatness of the reporter sphere and the mean phase error. The standard deviation of the electron density within the reporter sphere was divided by the standard deviation of the protein density. The mean phase error is plotted against this 'relative flatness'. Each data point corresponds to a different density-modification protocol after 20 cycles of density modification. The flipping factor and the way of recombining phases was varied, as well as the inclusion or exclusion of weighted or unweighted non-crystallographic symmetry averaging. When a protocol results in random phases, the relative flatness can become larger than 1 if the protein region, but not the reporter sphere, is averaged or truncated.

2.3. *Identification of heavy-atom derivatives*

Derivatives were initially screened on a laboratory source at 6.5 Å resolution. A complete data set could be collected from two to three positions of one crystal in 18 to 24 h. The data quality was such that single Hg sites were readily detectable in a difference Patterson (Fig. 1). We identified several isomorphous derivatives, but only methyl-mercury nitrate gave significant phase information beyond 7.5 Å. Fortunately, this one derivative, the two to three major sites of which are fairly well buried within the protein, was sufficient to solve the

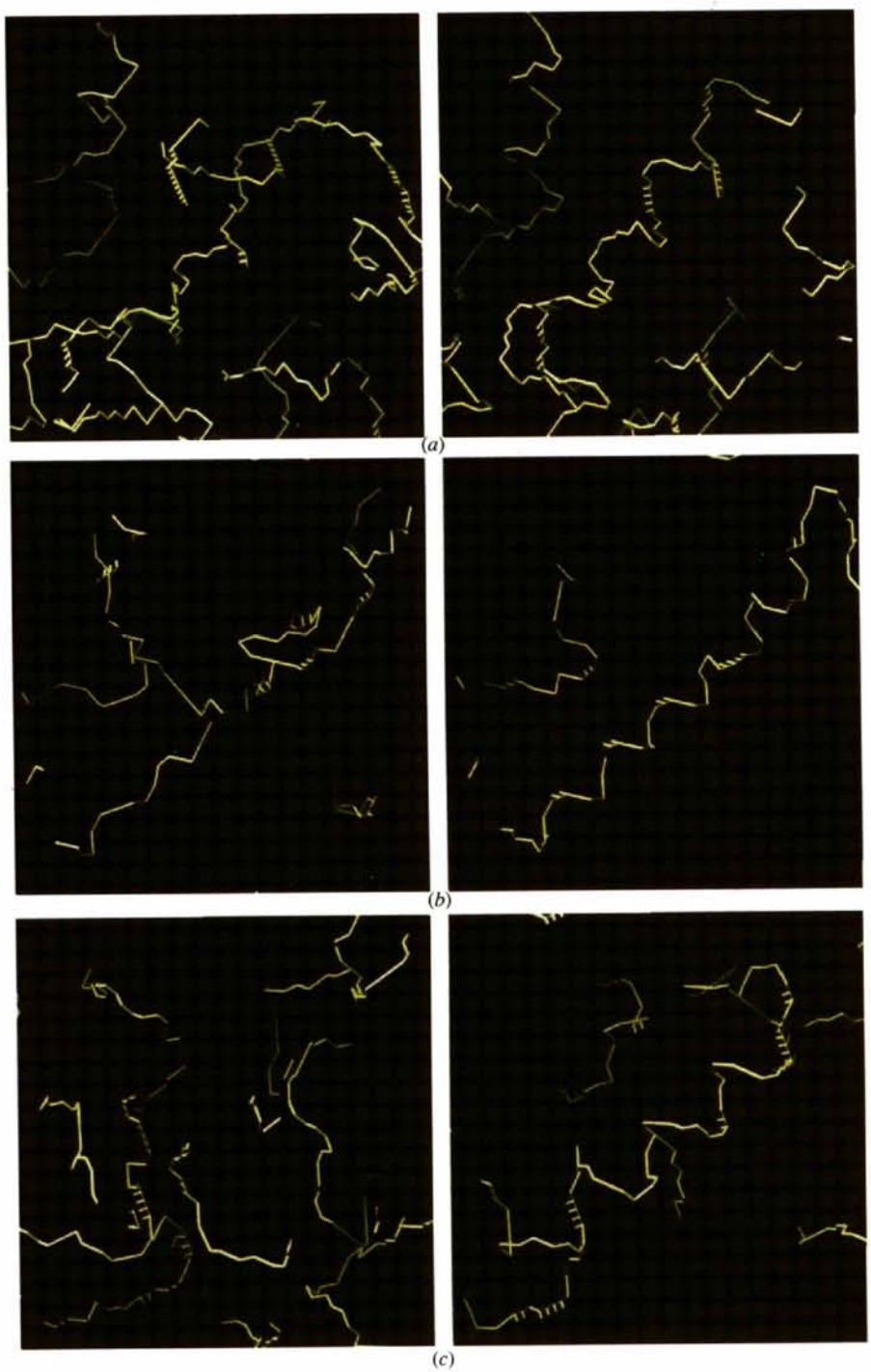

Fig. 6. Skeletonized representations of identical parts of electron-density maps before and after solvent flipping and truncating 40% of the protein volume, as described in the text. The integration radius for determining the LSD maps used for the solvent mask definition was set to the maximum resolution to which phase information was available. Non-crystallographic symmetry averaging was not applied in any of the examples. Phase improvement reveals the pitch in helices and removes false connectivities in sheet regions (not shown). (*a*) CytB, a mosquito toxin from *Bacillus thuringiensis* (courtesy of Dr J. Li). The experimental phase probability distributions were based on five poor derivatives. The solvent content was set to 33%. The initial mean phase error to 3 Å drops from 57 to 42° after density modification. (*b*) F_1 ATPase. The phase probability distributions were calculated from methyl-mercury derivatives as described in the text. The solvent content was set at 50%. The mean phase error drops from 56 to 36.5° after density modification. (*c*) CAT (see *Appendix*). The phase-probability distributions were calculated from an iodinated substrate derivative, which was highly isomorphous, but had a low signal. The solvent content was set to 50%. The mean phase error to 2.7 Å drops from 56.5 to 33.2° upon density modification.

Table 1. *Summary of the phasing statistics of the F_1 ATPase data set extending to 3.2 Å*

The crystals were soaked for 16 h in 0.2 m*M* methyl-mercury nitrate and their data were collected at station 9.6 at the SRS in Daresbury, UK, using a wavelength of 0.9 Å. Two other derivative data sets (statistics not shown) of crystals soaked in 1 m*M* and 0.2 m*M* methyl-mercury nitrate were collected to 3.5 Å resolution, using wavelengths of 0.92 and 1.54 Å, respectively. The quality of the native data has been adequately summarized in Abrahams *et al.* (1994). For each of the derivative data sets refined fractional coordinates of the sites are listed.

							Fractional coordinates of the sites		
							X	*Y*	*Z*
							0.592	0.241	0.210
							0.081	0.621	0.102
							0.059	0.094	0.192
							0.260	0.271	0.071
PhP_a*	PhP_c*	R_c†	R_d‡	R_m§	Cmp¶	Mult**	Refined occupancy, B††		
1.0	0.9	0.75	11.6	6.6	31.8	1.2	(0.58, 44); (0.48, 32); (0.05, −3); (0.03, −18)		
1.3	1.0	0.65	11.3	5.7	47.2	1.6	(0.58, 41); (0.52, 34); (0.05, 8); (0.04, −12)		
1.7	1.1	0.51	10.4	5.1	42.6	2.0	(0.65, 45); (0.58, 39); (0.84, 32); (0.28, 68)		
1.5	1.1	0.57	10.3	5.5	74.2	2.1	(0.60, 43); (0.58, 38); (0.11, 42); (0.28, 68)		
1.3	1.1	0.61	10.6	5.4	31.2	1.5	(0.56, 42); (0.57, 37), (0.10, 30); (0.24, 30)		
1.3	1.0	0.64	12.7	6.1	27.2	1.2	(0.63, 45); (0.59, 36); (0.14, 49); (0.01, −60)		

* PhP_a and PhP_c, the phasing power (the r.m.s. isomorphous difference divided by the r.m.s. residual lack of closure) of the acentric and the centric reflections, respectively. † R_c, the Cullis R factor: $\sum \big||F_{PH} - F_P| - |F_{H(calc)}|\big| / \sum |F_{PH} - F_P|$. Summed over centric reflections. ‡ R_d, $\sum \big||F_{PH}| - |F_P|\big| / \sum |F_P|$. § R_m, $\sum_h \sum_i |I(h) - I(h)_i| / \sum_h \sum_i I(h)_i$ where $I(h)$ is the mean intensity after rejecting observations deviating more than 3.5 standard deviations from the mean. The contributing reflections were weighted by their mean standard deviations, which were determined by adjusting the measured standard deviation to reflect the observed differences between symmetry-related reflections. ¶ Cmp, completeness. ** Mult, multiplicity. †† Refined occupancy and temperature factor of each of the sites.

structure to 2.8 Å resolution subsequently. A summary of the low-resolution data has been given by Abrahams *et al.* (1993).

The initial experiments at low resolution indicated that upon soaking the crystals in 1 m*M* methyl mercury instead of 0.2 m*M*, additional sites within F_1 become occupied. The total amount of additional substitution is relatively small, an increase from 2.4 to 3 Hg atoms per asymmetric unit containing about 30 000 ordered atoms (based on an occupancy of 1.0 for the mercury site with the highest substitution), but nevertheless this derivative provided useful additional phasing information.

2.4. *Determination of phase-probability distributions to 3.2 Å*

Because of the limited crystal lifetime, many crystals were needed for most high-resolution data sets. We found that the heavy-atom substitution could differ slightly but significantly between crystals, possibly due to somewhat different soak times. Therefore, the heavy-atom parameters of each individual derivative crystal were refined against the corresponding native data set using *MLPHARE* (Otwinowski, 1991). Intensity measurements of different derivative crystals were only merged if there were no significant differences in the refined occupancies and temperature factors of the heavy atoms of the individual crystals. Otherwise the crystals were treated as separate derivatives within *MLPHARE*. A drawback of this procedure is that the resulting phase probability distributions are artificially sharpened for reflections measured from different crystals. This overestimation of the quality of the phase information, which occurs when highly related derivatives are treated as fully independent ones, is caused by the similarity of the non-isomorphous component of corresponding structure-factor differences.

For all synchrotron data collected at a given wavelength, the anomalous occupancies were calculated from the mean ratio between refined real and anomalous occupancies of all the individual sites. A summary of the phasing statistics of the 3.2 Å data is given in Table 1. Note that none of the data from the low-resolution structure were used for solving the high-resolution structure, with the exception of the coordinates of the mercury sites with a high occupancy. The additional mercury sites were redetermined from a difference Fourier synthesis.

As mentioned above, the native data sets corresponding to the various derivative data sets were also significantly different from one another. The mean difference between the 'best' phases of the two synchrotron data sets was 61° (ranging from 50° in the low-resolution shells to 70° in the highest resolution bin). Similarly, the mean difference between the 3.2 Å synchrotron data and the data collected in the laboratory was 65° (ranging from 50 to 78°). Finally, the mean difference between the laboratory data and the 3.5 Å synchrotron data was 68° (ranging from 50 to 82°). In order to combine the phase information of the various data sets, corresponding Hendrickson–Lattman coefficients of equivalent reflections were added together. The combined data set inherited the structure-factor amplitudes from the data set which was measured to a resolution of 2.8 Å. The rationale for this procedure was that the systematic differences of the structure-factor amplitudes between the various data sets were probably much smaller than the uncertainties of the

phases, so that information was gained rather than lost. We preferred the combination in reciprocal space, rather than in real space through the addition of density maps, because in the latter case information on the bimodality of the phase probability distribution is lost.

The addition of Hendrickson–Lattman coefficients of related phase probability distributions again causes an artificial sharpening of the resulting distributions for reasons explained above. Before pair-wise combination, the coefficients of those reflections present in both contributing data sets, but not the coefficients of unique reflections, were, therefore, scaled down. The scaling factor was based on estimates of the independence of the phase information of the contributing data sets, and on estimates of the artificial sharpness of the distributions of the individual data sets.

The scale factors were set to 0.5, 0.75 and 0.5 for the 3.2 Å synchrotron data, the 3.5 Å synchrotron data and the 3.5 Å laboratory source data, respectively. Since these values produced maps of excellent quality, no other combinations of values were tried. The values should each have been set to 0.33 if the accuracy of the phase information was limited by non-isomorphism rather than the experimental error of the structure-factor amplitudes, if the contributing phase probability distributions were not too sharp and if these distributions had been derived from identical derivatives. The values used were higher than 0.33 because the derivatives are not identical and because we assumed that non-isomorphism does not fully limit the quality of phase information. However, we did not set each of them to 1, because the individual phase probability distributions were too sharp, and because it is likely that the non-isomorphous components of the structure-factor differences of the various derivatives are similar.

2.5. *Density modification*

In all density-modification procedures described below, structure factors calculated from modified maps were recombined with the experimentally determined phase probability distributions using σ_A weighting. Structure-factor amplitudes corresponding to the $(2|F_o| - |F_c|)$ values as returned by the *SIGMAA* program (Read, 1986) were used for calculating the next map of the iterative modification procedures. In most cases, convergence was reached within ten to 20 cycles. All maps were computed using data between 15 and 3.2 Å, the resolution range in which experimentally determined phase information was available.

Initially, maps were calculated using a previously described procedure for solvent flattening (Wang, 1985; Leslie, 1987). Inspection of skeletonized density allowed us to identify many elements of secondary structure. It quickly became clear that the structure of F_1 is asymmetric, so that in order to improve the phases by averaging, separate masks and symmetry operators would be needed for each of the three domains of both the α and the β subunits. Masks and symmetry operators were determined and refined using *O* and programs from the *RAVE* package (Jones, Zou, Cowan & Kjeldgaard, 1991; Kleijwegt & Jones, 1994). One of us (JPA) wrote a program, *Solomon*, which removes overlap between different masks and their symmetry copies, analogous to the procedure adopted in the *RAVE* package for removal of overlap between symmetry-related copies of a single mask. In this procedure, gridpoints lying at the edge of a mask are deleted if they fall within the region of another mask, and this process is iterated until all overlap has been removed.

Subsequently, *Solomon* was extended to read electron-density maps and average them using supplied masks and symmetry operators, using a single interpolation procedure. Because it was anticipated that the non-crystallographic symmetry was more exact in some parts of the masks than in other parts, a form of weighted averaging was implemented. In this procedure, the density at each grid point within a mask is compared pair-wise to the interpolated density at all non-crystallographically related points, calculated by fitting three-dimensional cubic splines. If the noise level of the map is known, the significance of the observed difference in electron density can be computed. The averaging is then weighted by the probability that the difference is accidental.* The program estimates the noise, which for simplicity was assumed to be of a uniformly Gaussian nature, from the standard deviation of a spherical 'monitoring' patch within the solvent. In order not to bias the estimate of the noise of the map, it is important not to modify the electron density within this reporter sphere during the density-modification procedure. Provided the phases improve, the errors in the map should decrease, and the solvent should get flatter. At the same time, small differences between non-crystallographically related parts become more significant, and averaging at these points should be weighted down.

In order to find a sphere suitable for monitoring the noise, the program determines the standard deviation of the electron density within a given radius relative to the overall mean at every gridpoint of an unmodified, figure-of-merit weighted electron-density map. This procedure produces a new map, describing the local standard deviation, an 'LSD map'. The grid point with the lowest value of the LSD map is then used as the centre of a mask, defining a 'reporter sphere'. We have only used a reporter sphere with a radius of 8 Å in the case of F_1 ATPase. The smaller the radius is, the less accurate the estimate of the errors of the map will be, because of

---

* Averaged density at a given gridpoint: $d_{av} = \sum(d_i/\mathrm{wgt}_i)/\sum(1/\mathrm{wgt}_i)$, where (d_i) is the density related by the ith symmetry operator and (wgt_i) is the corresponding weight $\mathrm{wgt}_i = 1 - 2/[(2\pi)^{1/2}\sigma]\int_0^{|z|/2^{1/2}}\exp(-z^2)\delta z$. In this equation $[z = (d - d_i)/\sigma]$, where (d) is the original density and (σ) is the standard deviation of the noise.

high-resolution ripples caused by discontinuities at the surface of the reporter sphere.

An LSD map is in fact the square root of a convolution of a sphere and the squared map, and it can, therefore, also be calculated in reciprocal space in a similar way to the procedure described by Leslie (1987). Especially when the integration radius is large, this will significantly improve the speed of calculation. However, when the radius is small, the real-space algorithm is also quite rapid, because neighbouring grid points will have a large part of their surroundings in common, thereby reducing the amount of computation required.

In a further extension of *Solomon*, the LSD maps were used to define the solvent envelope. Histograms of these maps show a bimodal distribution, reflecting the solvent content of the crystals (Fig. 2*a*). By integrating the histogram, the cut-off value of the local standard deviation corresponding to the solvent fraction can be calculated. To determine the solvent envelope, an initial high cut-off value is chosen, so that the number of gridpoints below this high cut-off corresponds to the solvent fraction and 50% of the protein fraction. This generous solvent mask is then modified recursively by removing gridpoints with values above the solvent cut-off, provided they are connected to an existing protein region. This procedure effectively removes islands of a high local standard deviation from the solvent region. Inspection of these masks revealed solvent envelopes of a very high quality, even when a radius as small as 3.7 Å is used for determining the local standard deviation (Fig. 2*b*).

The solvent envelope determined as described above can intrude into masks used for the averaging procedure. However, since this is not desirable in some cases, one can prevent the solvent mask from entering specified masks. In particular, the mask earmarked for the determination of the noise level of the map will be excluded from the solvent. On the other hand, masks can be specifically assigned to the solvent region as well. This can be used to specifically include ghost peaks of heavy atoms in the solvent mask, for example.

Using a solvent-flattened and averaged electron-density map, the trace of the main chains was determined with great ease from a skeletonized representation of the electron density, using *O* (Jones *et al.*, 1991).

Subsequently, an alternative method of modifying the electron density in the solvent region was investigated. For all grid points within the solvent the electron density was set to,

$$\rho' = \rho_{\text{avg}} + k_{\text{flip}} (\rho - \rho_{\text{avg}}),$$

where ρ_{avg} is the mean solvent density, ρ is the original density and k_{flip} is a 'flipping factor'. Conventional solvent flattening corresponds to a value of zero for the flipping factor. However, it was found that a significant improvement of the map was obtained by setting this value to -1, in other words, by flipping the features of the solvent. This observation, which initially was based on the reduction of noise as measured from the reporter sphere described above, was confirmed by inspection of the maps and at a later stage by comparing the resulting phases to those calculated from the refined model (Fig. 3).

2.6. *Map interpretation*

The maps derived from the 'solvent-flipping' procedure without averaging, were superior to those obtained using solvent flattening and non-crystallographic averaging, and were used to build the atomic model of F_1 ATPase. Later tests showed that even better phases can be obtained by combining averaging and flipping, after optimizing the flipping factor (Fig. 3).

The atomic model was built using the *baton* and *lego* options in '*O*' (Jones *et al.*, 1991). The methylmercury site at Cys251 in the α subunit was used as a marker when fitting the amino-acid sequence for this subunit, and the similarity in the fold of the α and β subunits allowed the homologous residue in the β subunit to be identified. It was frequently found that after automatically building both the main chain and the side chains, the positions of the Cα atoms could be improved by manually optimizing the fit of the side chains in the electron density. The improved positions of the Cα atoms then allowed another search in a database of known structures for a better fitting stretch. In more difficult regions, it was sometimes necessary to iterate this procedure a couple of times, but generally it allowed for a very quick and accurate interpretation of the density.

Practically all amino acids of the α and β subunits could be built into the density, but only part of the γ subunit could be fitted and the δ and ε subunits could not be traced at all. A map describing the local standard deviation indicates the presence of poorly ordered density around the area where the γ subunit protrudes from the main body of the particle. We assume that the disordered δ and ε subunits and the parts of the γ subunit which are not present in the current model, are located here.

2.7. *Structure refinement*

The structure was refined in *X-PLOR* (Brünger, 1993) and *PROLSQ* (*CCP*4, Collaborative Computational Project, Number 4, 1994), but no use was made of the simulated-annealing facilities of the former program. Only 95% of the data from 6 to 2.8 Å were used for the refinement, the remaining 5% were reserved for the structure validation as described by Brünger (1992). Although the maps were calculated using all the data, we only used data beyond 6 Å resolution for the refinement.

One of the reasons for doing so is the inadequacy of current programs of modelling very poorly ordered density, like that of the δ and ε subunits which are only visible as a slight increase in the local standard deviation of the map. The initial R factor was 40% for all data between 15 and 3 Å resolution. Following three rounds of rebuilding and refinement, the final R factor was 16.1% for all data between 6 and 2.8 Å, and the free R factor was 25.2% for the same resolution range. No non-crystallographic symmetry restraints were applied during the refinement.

3. Discussion

3.1. *Data processing*

It is unusual that a new structure as large as F_1 ATPase is solved using only one heavy-atom compound. The relatively small signal of just 2.4 to 3 Hg atoms in a structure of 372 kDa prompted us to collect and process the data with utmost care, ensuring both a high degree of completeness and a high multiplicity of observations. Each segment of derivative data, either from a new crystal or a new position on the same crystal, was initially treated as an independent derivative, and was only merged with other data if the refined heavy-atom parameters were in good agreement. This approach was important given the observed variation in heavy-atom substitution (Table 1). We also tried not to lose any information through small differences between derivative crystals, or indeed within the same crystal if the reaction with the heavy-atom reagent proceeded during data collection. The resulting phase probability distributions are artificially sharpened, but this can be corrected for, as explained above. Although we did not realise this at the time, it might be possible to refine the correction factor by minimizing the ratio between the standard deviations of the solvent and protein density of figure-of-merit weighted maps, analogous to the refinement of the flipping factor as illustrated in Fig. 3. It should be noted however, that using a resolution-independent correction as we employed, is only correct to a first approximation.

3.2. *Envelope determination*

The procedure for determining the molecular envelope based on the local standard deviation of the electron density allows the use of a smaller averaging radius than the 6 to 8 Å typically used in procedures derived from the one proposed by Wang (1985). Part of the reason for this is that in the former method all information present in the electron-density map is used, rather than just the features with a positive density. In the case of F_1 ATPase, an integration radius of only 3.7 Å could be used for determining the local standard deviation, resulting in a mask of relatively high resolution. Such a small radius can prove particularly valuable for surface protein loops, which may well be classified as belonging to the solvent region if an envelope of a relatively low resolution is used. The use of a small radius can lead to 'islands' of protein in the solvent region. These islands are reclassified automatically by the program as described earlier. Lakes of solvent in the protein region could be reclassified in a similar fashion, but we did not implement this option in view of the large internal cavity of F_1 ATPase. The accuracy of the envelope determined for F_1 ATPase is illustrated in Fig. 2(*b*).

It should be noted that it is more correct to determine the local standard deviation relative to the mean solvent density, rather than to the overall mean density of the map. In the maps of F_1 ATPase these two hardly differ, partly because of a low-resolution cut-off of 15 Å, but this is obviously not universally the case. Because of this, we included the option of adding a constant term to the map, through which the mean density of the solvent can be set to zero. When the diffraction data is incomplete, which causes ripples in the electron-density map, it might be more appropriate to determine the local standard deviation relative to the local mean. However, we did not implement this procedure.

The determination of the solvent mask is independent of the definition of protein masks which are used to define the non-crystallographic symmetry. This has the advantage that the boundaries of protein masks do not need to be defined very accurately, as long as they describe volumes in which the non-crystallographic symmetry is properly maintained. In practice this means that one can generate averaging masks which generously include solvent at their borders without reducing the volume which will be treated as solvent. The only consequence of doing so is that the solvent within these masks will be averaged before it is flipped. On the other hand, parts of the protein which do not obey non-crystallographic symmetry do not need to be included in unique masks, since they will not be treated as solvent, provided that these regions are recognized as protein in the LSD map.

3.3. *Solvent flipping*

Estimates of phases from an initial set of experimentally determined phase probability distributions, $\{P_o\}$, can be improved by imposing additional restraints provided by correct information about the structure (reviewed by Drenth, 1994). In practice, restraints like solvent flatness and non-crystallographic symmetry are most easily applied in real space by modifying a figure-of-merit weighted electron-density map, rather than in reciprocal space by combining structure-factor probability distributions.

From the difference between the structure-factor amplitudes $\{|F_c|\}$ derived from the modified map and the observed structure-factor amplitudes $\{|F_o|\}$, the proba-

bility distributions around the modified phases, $\{P_c\}$, can be calculated. In practice, these new probability distributions indicate how well the unmodified map adheres to the restraints to which it was subjected. By combining $\{P_c\}$ and $\{P_o\}$ a new phase probability distribution can be calculated, allowing the computation of a new figure-of-merit weighted density map. This new map can then be subjected to similar restraints. The recombination of $\{P_c\}$ with $\{P_o\}$ represents a major contribution to the success of density-modification procedures, especially in the absence of non-crystallographic symmetry restraints. If during the iteration new maps are calculated from the unrecombined phases of the modified maps and $\{2|F_o| - |F_c|\}$ amplitudes, the mean phase error after optimizing the value of the flipping factor is 49° instead of 37.6° in the case of F_1 ATPase, for which the initial phase error was 56°. Although symmetry constraints lessen the difference, recombination remains beneficial: if partial threefold symmetry is imposed on maps of F_1, the mean phase error can be reduced to 39° without, and to 33.2° with phase recombination.

A major problem associated with the procedure is to calculate $\{P_c\}$, or, what is essentially equivalent, to determine the weight of $\{P_c\}$ when combining it with $\{P_o\}$. The problem is caused by the difficulty of assessing the quality of the modified map in the absence of additional independent knowledge about the structure. The multitude of weighting schemes in use indicates the general unease felt about this problem (Sim, 1960; Rayment, 1983; Read, 1986; Grimes & Stuart, 1994).

The scheme we employed calculates $\{P_c\}$ from the difference between $\{|F_o|\}$ and $\{|F_c|\}$, assuming that the latter is derived from an independent, incomplete and inaccurate model. This procedure, proposed by Srinivasan & Ramachandran (1965) has been implemented by Read (1986) in the *CCP*4 program *SIGMAA*. However, it has been observed that it overestimates the quality of $\{P_c\}$ if $\{|F_c|\}$ is not independent of $\{|F_o|\}$ (R. Read, personal communication). In density-modification procedures, $\{|F_c|\}$ is derived directly from $\{|F_o|\}$ and the assumption that the two are independent will only become valid if the restraints imposed on $\{|F_o|\}$ to produce $\{|F_c|\}$ are strong enough. The overestimation of the weight tends to be more severe when $\{||F_o| - |F_c||\}$ is small, in which case the procedure can only assume that, therefore, the phases must be almost correct, something which is not necessarily the case. Compare for example a case in which only 20% of the map is flattened with a case in which 12-fold symmetry is imposed in addition to solvent flatness. If in the latter case $\{|F_o|\}$ and $\{|F_c|\}$ are similar, then this is a good indication that the phases are virtually correct. However, in the former case such a similarity between $\{|F_o|\}$ and $\{|F_c|\}$ is more likely to reflect the fact that only a small proportion of the map was changed. Solvent-flattening procedures are prone to converge prematurely, because the inflation of the weight of $\{P_c\}$ is fed back into the new $\{F_c\}$ of the next cycle, making the new $\{||F_o| - |F_c||\}$ even smaller. This shows up as a rapid inflation of the figure of merit, for example.

A possible reason for the success of the solvent-flipping procedure as described in the *Methods* section, now becomes apparent. At resolutions where the solvent does not contribute to the scattering, the procedure is essentially equivalent to over-shifting the structure-factor changes implied by the restraints. By applying the extra shift, $\{|F_c|\}$ usually becomes more different from $\{|F_o|\}$ and because of this, the weight of $\{|F_c|\}$ is not overestimated as much and the rapid inflation of the figures of merit upon iteration of the procedure is kept in check.

Another reason for the success of the solvent-flipping procedure is to be found in a side effect of the recombination of the modified phases with $\{P_o\}$. Though this recombination is virtually essential unless one can average over a large number of copies, it does have the tendency to dampen the phase shift, since it biases the resulting phase probability distribution to that of the initial map. By exaggerating the shift, the dampening can be neutralized to a greater or lesser extent. The beneficial effects of the recombination, like the discrimination between well and poorly phased structure factors, are maintained and a larger part of phase space is explored. Although the dampening of the phase shifts can also be overcome by increasing the weight of $\{P_c\}$, this would not be desirable since it would be accompanied by the artificial inflation of the figures of merit described earlier.

The exaggeration of the structure-factor shift will also tend to make $|F_c|$ more different from $|F_o|$ for those structure factors which undergo a large phase change upon modification. The P_c of these poorly determined or ill fitting structure factors will, therefore, usually be down weighted more by applying the extra phase shift, compared to better fitting structure factors.

The effects of solvent flipping in conjunction with phase recombination are that the weight of the modified phases is decreased, that the phase change is increased, so that a larger part of phase space is explored, and that the discrimination between poorly determined and well determined structure factors is enhanced. The tests presented here clearly demonstrate that density-modification procedures can significantly benefit from these effects.

In iterative density-modification procedures the phases are alternately subjected to restraints in real space, where the density is modified using chemical knowledge, and to restraints in reciprocal space, where these modifications are tested against the experimental data. It is the combination of the two faces of the procedure which determines its final success. Modifying electron density in a way which does not seem to make chemical sense can still be of benefit if it results in an improvement of the part of the procedure taking place in reciprocal space. Conversely, modifying electron density in a way which does make chemical sense can be detrimental if it decreases the validity of some

of the assumptions in reciprocal space. It is, therefore, dangerous to judge the validity of a procedure by only arguing its chemical justification.

3.4. *Averaging and truncation*

Other ways of enhancing the benefits of solvent flattening are in wide use. For example, a certain fraction of the protein density can be truncated by setting every gridpoint within the protein region with an electron density below a certain value to this value (Schevitz, Podjarny, Zwick, Hughes & Sigler, 1981). Alternatively, the variation of electron density within the protein region can be modified to reflect the theoretical variation through histogram-matching procedures (Zhang & Main, 1990). Both these additional restraints are inspired by correct information about protein structures, and in the first case practical considerations usually require somewhat arbitrary decisions on the level of truncation, while in the second case the resolution of the phase information needs to be sufficiently high. We established that the beneficial effects of truncating a fraction of up to 40% of the protein density are to a certain amount independent of the solvent-flipping procedure: in the case of F_1 another 2° of phase improvement to a mean error of 35.5° is feasible. The optimum solvent-flipping factor increases from −1.0 to −0.8 in this case (see Fig. 3*b*). Over truncation fractions varying from 0 to 50%, the magnitude of the optimal flipping factor is highly correlated with the reduction in variance of the protein region resulting from the truncation. This means that once an optimum flipping factor has been determined at a given truncation level, the best flipping factor at other truncation levels can be determined automatically. We think it is likely that techniques which require the availability of data to a higher resolution, like histogram matching and possibly skeletonization (Baker, Bystroff, Fletterick & Agard, 1993), will also still exhibit their beneficial effects in concert with the solvent-flipping procedure.

Figs. 3(*c*) and 3(*d*) clearly demonstrate that the results of flipping the solvent can be improved by additional non-crystallographic averaging. Since it was clear that the symmetry of the F_1 ATPase particle is not exact, we also implemented a form of locally weighted averaging as described in the *Methods* section above. However, the differences between weighted and unweighted averaging are subtle and both perform about equally well in reducing the phase error in the case of F_1 ATPase.

In those resolution shells where the solvent does not contribute to the Bragg scattering, solvent flipping is equivalent to overshifting the structure-factor difference in reciprocal space after solvent flattening. The procedure can, therefore, also be performed in reciprocal space. In practice this is done by applying a Fourier transform to a set of structure factors, modifying the resulting map and back-transforming it. After determining the complex structure-factor differences between the initial and the modified structure factors, these are subtracted (after scaling by the flipping factor) from the modified structure factors. If, in addition to modification of the solvent density, non-crystallographic symmetry constraints are introduced, such a general exaggeration of the shifts in reciprocal space is essentially equivalent to simultaneously flipping the solvent and increasing the overall weight of symmetry-related density with respect to the original density during the averaging in real space. In a test we performed on F_1 ATPase in which a partial threefold non-crystallographic symmetry was imposed strictly, such a general exaggeration of the shifts in reciprocal space proved slightly inferior to only overshifting the contribution of the solvent modification, but not that of the averaging. In this case the mean phase error is reduced to 34.1° in the former, and to 33.2° in the latter case. However, if the averaging is locally weighted according to the procedure described in the *Methods* section, the general overshifting of the structure-factor differences is slightly superior to restricting the extra shift to the solvent fraction. Now the mean phase error is reduced to 32.9° in the former, and 33.3° in the latter case (see also Fig. 4). It is unclear however, to what extent these differences are significant.

If in addition to solvent flipping and non-crystallographic averaging, the protein density is also truncated, the mean phase error is not further decreased in the case of F_1 ATPase. However, there are clear indications that such a combination can be beneficial in other cases.

The combination of the solvent-flipping procedure with non-crystallographic averaging and truncation of negative density requires optimization of some parameters (the flipping factor, the solvent content, the averaging radius and the truncation level, for example). To a certain extent the optimal flipping factor is correlated to the solvent content (the less solvent, the more negative k_{flip}) and to the amount of non-crystallographic averaging (the more averaging, the less negative k_{flip}). If the correct structure is not known, another measure of the quality of the modified maps is required. For this purpose, we introduced the flatness of an unmodified area of solvent, the reporter sphere, as such a measure. This procedure is closely related to the calculation of 'omit' maps, which are used to identify model bias. Instead of leaving out part of the data, as in free *R*-factor calculations (Grimes & Stuart, 1994), not all the information about the structure is used for the refinement of the structure factors by density modification, thus allowing an independent validation of the result. There is a good correlation between the flatness of the reporter sphere and the mean phase error (see Fig. 5). One possible problem associated with a straightforward adaptation of the procedure described in the *Methods* section, is that if the solvent cavities are small, it might be difficult to identify a suitable spherical volume. In such

cases it might be better to look for a sphere furthest away from the volume occupied by the protein. The single value of the flatness of the reporter sphere cannot convey information about the resolution dependency of the phase errors. A Fourier transform of the patch might allow one to extract such information.

We did not anticipate that it would be possible to solve the structure of F_1 ATPase using just a single heavy-atom compound without the use of non-crystallographic symmetry. The initial mean phase error of 56° can be improved by as much as 23°, but only 2.5° of this improvement can be attributed solely to non-crystallographic averaging. The best phases result from overshifted weighted averaging and partially flipping the solvent simultaneously, in which case the mean phase error can be reduced to 32.9°, compared to 33.2° if solvent flipping is combined with unweighted averaging. This should be compared to a minimum phase error of 35.5° which results from just flipping the solvent and truncating 20% of the protein region, while the phase error is 35.4° if the map is averaged, and if the solvent is flattened rather than flipped. If the solvent is flattened without averaging or truncation, the mean phase error is 44.6°.

The highly isomorphous derivative, the use of synchrotron radiation and image-plate detectors, the careful data processing and the new density-modification procedures described in this paper all were essential components of the successful structure determination of the F_1 ATPase particle.

4. APPENDIX
Further evaluation of the density-modification procedures

In order to assess the general validity of two novel aspects of the density-modification procedure, namely solvent flipping and the definition of the solvent envelope based on the local standard deviation, additional tests were carried out using chloramphenicol acetyltransferase (CAT) as a model system. CAT is a trimer (subunit $M_r = 25\,000$) which crystallizes in space group $R32$ (hexagonal cell parameters $a = 107.6$, $c = 123.4$ Å) with a monomer in the crystallographic asymmetric unit. The structure has been refined at 1.75 Å resolution, with a final R factor of 15.9% (Leslie, 1990). Tests were carried out using three different starting phase sets. The first is based on an iodinated substrate derivative (PICM), the second on a gold cyanide derivative (AuCN) and the third on the combination of the PICM and AuCN derivatives. In all cases the anomalous scattering contribution was included in the phase calculation. The phasing statistics are summarized in Table 2. The effect of solvent flipping alone was evaluated using the density-modification programs of the *CCP*4 suite, while *Solomon* was used to test the combination of the modified envelope determination and solvent flipping for the PICM derivative alone.

Table 2. *Derivative phasing statistics for the CAT test data (10–2.7 Å resolution)*

The native data is 99.3% complete between 20 and 2.7 Å.

	PICM‡	AuCN§	PICM+AuCN
m*	0.31	0.44	0.56
R_c†	0.61	0.49	
Completeness (%)	98	99	99

* Mean figure of merit. † Cullis R factor, $R_c = \sum ||F_{PH} - F_P| - |F_{H(calc)}|| / \sum |F_{PH} - F_P|$. ‡ PICM, *para*-iodo chloramphenicol. § AuCN, gold cyanide.

4.1. *Solvent flipping with the CCP4 suite*

The program *FLATMAP* in the *CCP*4 program suite (Collaborative Computational Project, Number 4, 1994) was modified to allow both solvent flipping and solvent flattening, adding k_{flip} as an input parameter. All data between 20 and 2.7 Å were used in the density modification. However, as there was no derivative information between 20 and 10 Å resolution, the phases calculated from the density modification were used with the observed structure-factor amplitudes in this resolution range. The solvent envelope was determined using the FFT implementation of the Wang algorithm (Wang, 1985; Leslie, 1987). A new envelope was calculated on every cycle. The *CCP*4 program *SIGMAA* (Read, 1986) was used for phase combination. Map coefficients $2mF_o - DF_c$ as output by *SIGMAA* were used to calculate the electron-density map for the next round of density modification. The success of the procedure was assessed by calculating the mean phase difference between the final phases and those calculated from the refined atomic model for reflections in the resolution range 10–2.7 Å.

4.1.1. *Protocols.* As in the case of F_1, a significant phase improvement was achieved by doing a final cycle of solvent flattening after multiple cycles of solvent flipping. When using the *CCP*4 programs, further improvement in the phases was obtained by performing additional cycles, alternately flipping and flattening the solvent. The final protocol used consisted of five cycles of flipping followed by two cycles of flattening, then two cycles flipping, then one cycle flattening, one cycle flipping and a final flattening cycle. The final phase error was insensitive to the number of cycles in the intermediate rounds, but it was important that the procedure finished with a single flattening cycle.

For the solvent-flattening tests, a total of six cycles were used.

When using *Solomon*, which determines a solvent mask based on an LSD map and optimizes the value of k_{flip}, the intermediate flattening cycles are not necessary.

4.1.2. *Parameter optimization.* The parameters that require optimization are the averaging radius used to

Table 3. *Mean phase difference (°) between the experimental phases and those calculated from the refined model of CAT*

For each phase set, the phase difference quoted represents the best result obtained, and the corresponding parameter values used in the density modification are given.

		Phase difference following density modification		Optimum parameter values			
				Flattening		Flipping	
Phase set	Initial phase difference	Flattening	Flipping	R_{env}* (Å)	Trunc† (%)	R_{env}* (Å)	Trunc† (%)
PICM	56.5	44.9	35.2	8	30	6	30
PICM (*Solomon*)	56.5		32.2			2.7	40
AuCN	52.9	38.6	31.5	6	30	6	30
PICM+AuCN	42.0	30.0	26.6	6	30	6	30

* R_{env}, averaging radius used in determination of the molecular envelope. † Trunc, percentage of grid points within the protein region at which the electron density was truncated.

determine the envelope and the parameter that determines the extent of truncation of density within the protein envelope. The parameters were optimized by minimizing the calculated phase error.

When using the *CCP*4 programs, averaging radii of 5, 6, 8 and 10 Å were used, and for each radius approximately 10, 20 and 30% of the grid points in the protein region were truncated. The parameter values giving the lowest phase error were selected. The solvent content was set to 50% (the estimated solvent content is 55%).

In the tests with *Solomon* the solvent content was set to 50%, the truncation level was set to 40% (but values between 20 and 45% produced very similar phasing statistics), the radius for determining the solvent envelope was set to 2.7 Å, the maximum resolution to which experimental phase information was available, and the flipping factor of −1 was scaled on every cycle by the reduction in variance of the electron density in the protein region due to truncation.

4.1.3. *Results.* For all three starting phase sets the solvent-flipping procedure provides a dramatic phase improvement, substantially greater than the more conventional solvent-flattening approach (Table 3). The improvement is most dramatic for the iodinated substrate derivative (PICM) where solvent-flattening results in a 12° phase improvement compared with 22° from solvent flipping. As the quality of the initial phase set improves, the overall reduction in phase error decreases, and the additional improvement of solvent flipping over solvent flattening becomes less apparent.

The success of the density modification is critically dependent on the completeness of the data. If 10% of the native data is removed (resulting in a completeness of 89%), the final phase error for the PICM derivative is 48.1° for solvent flattening and 47.5° for solvent flipping.

The alternative envelope definition procedure and the optimization of k_{flip} employed by *Solomon* produced a final phase error 3° smaller than that obtained with the *CCP*4 programs (Table 3).

The effect of the phase improvement on the interpretability of the electron-density maps is illustrated for three different examples in Fig. 6.

References

Abrahams, J. P., Lutter, R., Leslie, A. G. W. & Walker, J. E. (1994). *Nature (London)*, **270**, 621–628.

Abrahams, J. P., Lutter, R., Todd, R. J., Van Raaij, M. J., Leslie, A. W. G & Walker, J. E. (1993). *EMBO J.* **12**, 1775–1780.

Baker, D., Bystroff, C., Fletterick, R. J. & Agard, D. (1993). *Acta Cryst.* D**49**, 429–439.

Boyer, P. D. (1994). *Biochim. Biophys. Acta*, **1140**, 215–250.

Brünger, A. T. (1992). *Nature (London)*, **335**, 472–475.

Brünger, A. T. (1993). *X-PLOR Version* 3.1 *Manual.* Yale University, New Haven, CT, USA.

Collaborative Computational Project, Number 4 (1994). *Acta Cryst.* D**50**, 760–763.

Drenth, J. (1994). *Principles of Protein X-ray Crystallography*, pp. 189–198. New York: Springer Verlag.

Grimes, J. & Stuart, D. (1994). *From First Map to Final Model*, pp. 67–76. Warrington: Daresbury Laboratory.

Jones, T. A., Zou, J. Y., Cowan, S. W. & Kjeldgaard, M. (1991). *Acta Cryst.* A**47**, 110–119.

Kleywegt, G. J. & Jones, T. A. (1994). *From First Map to Final Model*, pp. 59–65. Warrington: Daresbury Laboratory.

Leslie, A. G. W. (1987). *Acta Cryst.* A**43**, 134–136.

Leslie, A. G. W. (1990). *J. Mol. Biol.* **213**, 167–186.

Leslie, A. G. W. (1992). In *Joint CCP4 and ESF-EACMB Newsletter on Protein Crystallography*, Vol. 26. Warrington: Daresbury Laboratory.

Lutter, R., Abrahams, J. P., Van Raaij, M., Todd, R. J., Lundquist, T., Buchanan, S. K., Leslie, A. G. W. & Walker, J. E. (1993). *J. Mol. Biol.* **229**, 787–790.

Otwinowski, Z. (1991). *Isomorphous Replacement and Anomalous Scattering*, pp. 80–86. Warrington: Daresbury Laboratory.

Rayment, I. (1983). *Acta Cryst.* A**39**, 102–116.

Read, R. (1986). *Acta Cryst.* A**42**, 140–149.

Schevitz, R. W., Podjarny, A. D., Zwick, M., Hughes, J. J. & Sigler, P. (1981). *Acta Cryst.* A**37**, 669–677.

Sim, G. A. (1960). *Acta Cryst.* **13**, 511–512.

Srinivasan, R. & Ramachandran, G. N. (1965). *Acta Cryst.* **19**, 1008–1014.

Wang, B. C. (1985). *Methods Enzymol.* **115**, 90–112.

Zhang, K. Y. J. & Main, P. (1990). *Acta Cryst.* A**46**, 377–381.